International Journal of Heat and Mass Transfer 52 (2009) 2871–2884

Contents lists available at ScienceDirect

International Journal of Heat and Mass Transfer

journal homepage: www.elsevier.com/locate/ijhmt

Investigation on thermal radiation spectra of coal ash deposits

Aleksandar Saljnikov [a,*], Mirko Komatina [a], Vasilije Manović [b], Milan Gojak [a], Darko Goričanec [c]

[a] Faculty of Mechanical Engineering, University of Belgrade, Kraljice Marije 16, 11120 Belgrade 35, Serbia
[b] CANMET Energy Technology Centre, Natural Resources Canada, 1 Haanel Drive, Ottawa, Ont., Canada K1A 1M1
[c] Faculty of Chemistry and Chemical Engineering, University of Maribor, Smetanova 17, Maribor 2000, Slovenia

ARTICLE INFO

Article history:
Received 7 October 2008
Available online 11 February 2009

Keywords:
Thermal radiation
Spectroscopy
Coal ash deposit
Temperature
Wavelength

ABSTRACT

This paper deals with thermal radiation properties of ash deposits on a pulverized coal boiler of an electric power plant. Normal emittance spectra in the 2.5–25 μm interval, and total normal emittance, were measured on 4 kinds of ash layers of a mm magnitude order thickness, at 560 → 1460 → 560 K in heating and cooling. It was found that ash powder layers are opaque for infrared radiation. The emittance increases with ash radiation wavelength and temperature. Ash powder is sintered and fused above 1200 K. The emittance of the sintered layer is above that of the unsintered layer. The authors propose, and explain by an example, correlating the experimentally obtained emittance spectra of ash deposits with a continuous curve, the formula of which defines the dependence of emittance on wavelength and temperature, i.e. $\varepsilon = \varepsilon(\lambda,T)$. Use of this formula, with parameter values determined by the proposed methodology, may greatly simplify the practical application of the experimentally determined emittances in the thermal design of existing and new steam boiler furnaces.

1. Introduction

In thermal design of a power plant boiler, in which pulverized low quality coal is used as the fuel, knowledge of thermal radiation characteristics of ash is important, since flying ash is deposited on the boiler walls and decreases the boiler efficiency.

Ash deposits are non-metallic materials. Thermal radiation characteristics of such materials greatly differ from those of metallic walls of the furnace, i.e. the surfaces of heat exchanger pipes in the boiler furnace. Because the real surfaces, by their non-homogeneity and structure, differ from the ideal surfaces as well – it is practically impossible to quantify the influence that deposits exert upon the heat transfer, by using the analytic tools. Therefore, this problem is predominantly solved by utilizing the experimental methods in order to determine the thermal radiation characteristics of deposits, concretely – their emittance and (less often) their absorptance.

There have been several works done on thermal radiation characteristics of ash deposits. Boow and co-workers [1] described their research for determining the emittance of deposits formed in lignite combustion at temperatures up to 1450 K. The measurement of total hemispherical emittance was done at 550–1450 K in the $\lambda = 0.13$–9.5 μm wavelength range, and of a spectral value at $\lambda = 0.9$ μm. It was concluded, and later confirmed by other authors [6,7,9,11,16], that the analyzed quantities strongly depend on temperature and on the thermal history of the material. It was observed (see Fig. 1) that ε^{total} decreases from 0.86 (at 550 K) down to 0.58 (at 1200–1300 K). The following temperature increase (1300–1450 K), leads to the sintering and later fusion of ash deposits, ε^{total} starts to increase and reaches ≈0.75 (at ≈1450 K). In cooling, ε^{total} rises continually, to ≈0.88 (at ≈560 K).

Spectral (monochromatic) emittance at 0.9 μm behaves similarly vs. temperature but the absolute values are lower. The values and temperature variation of emittance for the solidified slag taken from the combustion chamber were similar to those for the friable deposit after fusion. Besides the dependence of deposit emittance on temperature, it was concluded that this quantity strongly depends on the irreversible physical changes occurring at about 1100 °C and above.

In the subsequent article of Mulcahy et al. [2], the authors went a step further. Measurements of the thermal properties of a fusible boiler deposit, reported in [1], were used to calculate the overall effect of the deposit on the heat transfer to the water walls of the combustion chamber of a boiler fired with pulverized fuel. The chamber (furnace) is considered to be a continuous well-stirred reactor operated at constant energy input, and at any particular stage of deposition the same thickness of material is assumed to be present on the entire heating surface. The calculations are made for thicknesses of deposit varying from zero to steady maximum determined by the flow properties of the deposit. In the particular case considered, the flow point of the deposit material is about 1250 °C and the calculated maximum thickness of partially molten

* Corresponding author. Tel.: +381 11 3302 354; fax: +381 11 3370 364.
E-mail address: asaljnikov@mas.bg.ac.yu (A. Saljnikov).

0017-9310/$ - see front matter © 2009 Elsevier Ltd. All rights reserved.
doi:10.1016/j.ijheatmasstransfer.2008.12.007

Nomenclature

A, B	system constants for optical measurements,
C_2	Planck's second radiation constant (=0.014388 m K)
p	slope of the inclined part of the fitting line
t	thickness of specimen layer, m
T	temperature, K

Greek symbols

ε	radiation emittance
ε_{max}, ε_{min}	emittance asymptotes of the fitting line
λ	wavelength of radiation, μm
λ_m	wavelength of the mid-slope of the fitting line, μm
v	output of optical measurement system
ρ_p	heaping mass density of specimen layer, kg/m^3

Subscripts

B	blackbody
H	hemispherical
i(j)	corresponding to each wavelength (temperature) point
N	normal
room	room temperature
S	specimen

Superscripts

2.5–25 μm	spectrally-integrated over λ = 2.5–25 μm region
total	over the whole spectrum

deposit about 1 cm. Such a deposit produces a heat transfer drop of ≈40% from that obtained with clean tubes under otherwise equal conditions. A 0.05 cm layer of unfused deposit, as would normally be obtained in a few hours' operation of the boiler, reduces the heat transfer by about 7%.

The article [3] is the continuation of the articles [1,2]. It describes the testing of different materials with the aim of determining the physical–chemical properties that affect the total hemispherical emittance. The goal of that work was to determine the importance of the effect that – particle size (diameter *d*), heat radiation absorption coefficient (a), chemical composition, distance between the particles and degree of sintering – exert on ε. Tests were done on synthetic and natural combustion deposits from Australian coals, and ε was measured in the temperature interval 200–1200 °C.

It was concluded that ε^{total} increases – following the growth of absorption coefficient and particle size – until 400 μm (Fig. 2), whereas the particle size distribution depends upon the conditions in boiler under which the deposits are formed and collected, and their thermal history, as well as upon the structure and distribution of inorganic ash forming constituents. Chemical composition modifies the emittance results in two ways: (i) the presence of coloring agents, such as C and Fe, increases the absorption in the relevant wavelength regions and (ii) composition, together with the particle size, influences the temperature of onset of sintering and the fusion properties. For samples consisting of smaller particles the onset of sintering is at lower temperatures.

The authors of [4] conducted the experiments in order to determine total normal emittance of powdered ash deposits of different Russian coals in the 200–1000 °C interval, solely during sample heating. Emission intensity of the sample was compared with that of the blackbody. Sample surface temperature was measured by micro thermocouples, and at temperatures above 800 °C it was controlled by optic pyrometry.

For thin ash layers, possibility of radiation transparence was considered. To get an insight, the authors chose two types of vessels to place the samples: pyro-resistant steel and ceramics. The obtained plots, i.e. the experimental values of emittance, in the cases of different vessels, for ash thickness 0.8–1.0 mm, agreed well, so it had been concluded that layer that thick is opaque for thermal radiation. The experimental results obtained in this way, for the ash deposits from combustion of different Russian coals taken at the tube walls in boiler furnaces, have shown that heating of the ash sample does reduce its total emittance from roughly 0.8 at 300 °C to about 0.7 at temperature about 950 °C.

The authors of [5] were, as well, determining the total emittance of some Russian coals. The experiments were lead in the 530–900 K temperature interval. Similar results to those reported in [4] were obtained. The experimental set-up did permit the positioning of the radiation detector with the angle −60 to +60° from zenith, in vertical plane. That enabled determining the total directional emittance for this range of directions.

The obtained values of total directional emittance of ash deposits were averaged and that yielded values of total hemispherical

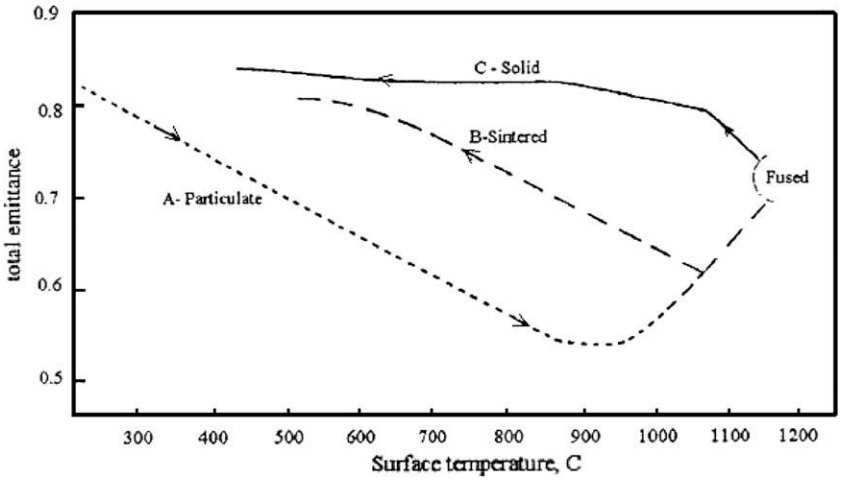

Fig. 1. Total hemispherical emittance of ash deposit vs. temperature [1].

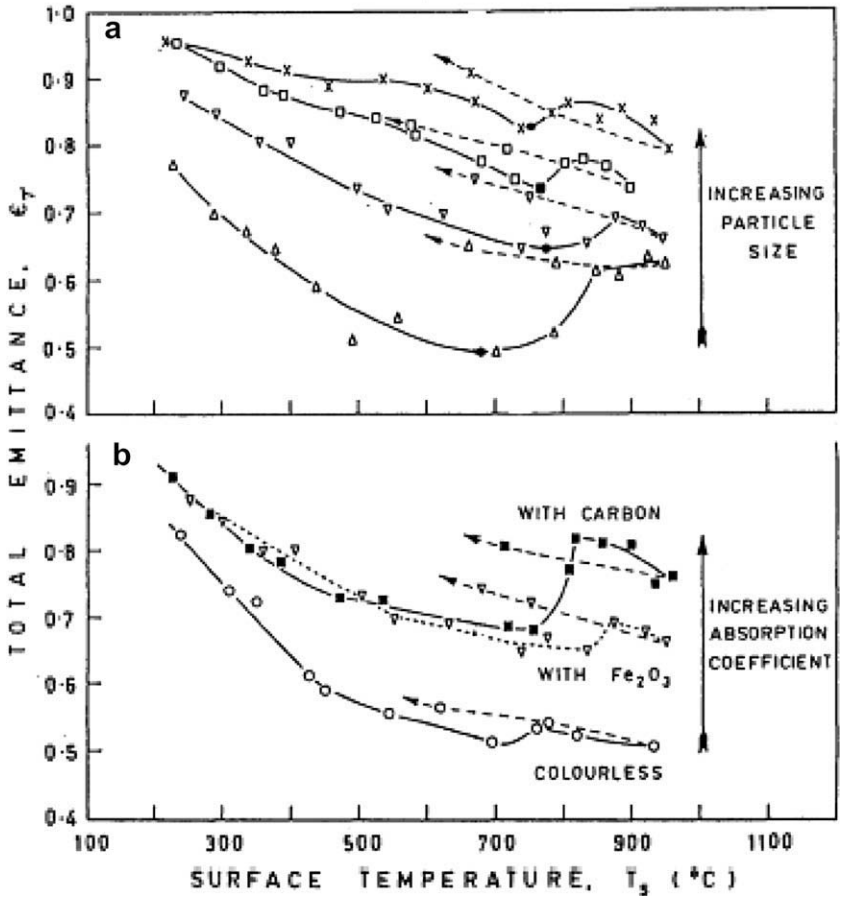

Fig. 2. (a) Effect of particle size on ε^{total} of synthetic slags with 5% Fe_2O_3 [3]. (b) Effect of "color" on ε^{total} of synthetic slags w. 53–104 μm particles [3].

emittance that were subsequently compared with the total normal emittance. This had resulted in clarifying the relationship of these two quantities. Based on measurements, performed with different Russian coals, it was found that the ratio of total hemispherical and total normal emittance is nearly 0.93.

Article [6] outlines the research on total normal, ε_N, as well as total directional emittance, ε_θ for five deposits of Serbian lignite. The values of the total normal emittance were determined for several commercial powders of the compounds that are included in the composition of real ash deposits: ferric oxide (Fe_2O_3), calcium sulphate ($CaSO_4$), sodium sulphate (Na_2SO_4), silica (SiO_2), alumina (Al_2O_3), as well as of their certain mixtures that were 1, 3 and 5 mm thick, within the 570–1270 K temperature interval. The directional emittance was measured in directions i.e. angles from −60° to +60° to zenith, at 773 K by using the total radiation flux meter. The authors of the articles have observed a significant drop in the values of total normal emittance with the temperature rising until 1000 K (Fig. 3). The sample was powdered deposit – taken from the furnace. A further temperature increase results in an emittance rise, particularly for the samples 1 and 3 mm thick – caused by the sintering, and subsequent fusion, of the deposit material. All these tested samples demonstrated a pronounced hysteresis. They were opaque, that was different to some deposit ingredients: sodium sulphate (Na_2SO_4) and alumina (Al_2O_3) that were semi-permeable and silica (SiO_2) which was opaque for the infrared radiation.

To relate the radiative properties and heat conductance of deposits, with physical and chemical properties easily observed or measured, a review [7] was made. The liaison between the theory and real data was analyzed for the first time, i.e. the spectral values of real indices of refraction and absorption, measured at room temperature

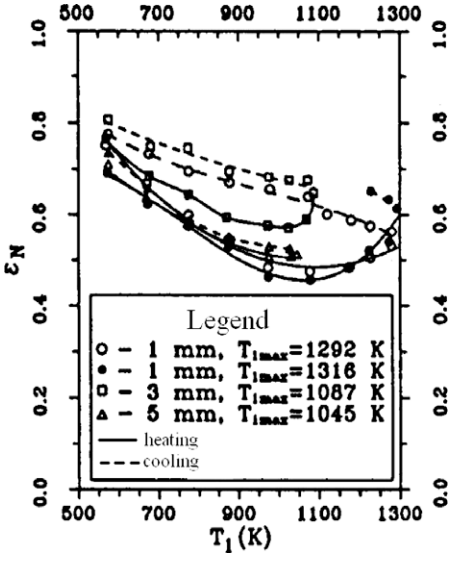

Fig. 3. Total emittance vs. temperature of a powdered ash deposit sample [6].

for 4 synthetic materials, of composition similar to real slag [8]. Spectral absorptance was determined from experimental data (by Mie theory) and the total emittance of ash particles, as well.

Articles [9,10] describe the measurement of spectral emittance of the ash deposits done by the FTIR spectroscopy on ashes of two different types of American coals (in Fig. 4 – data for one coal) in a pilot set-up during the initial 3 h of operation, starting from com-

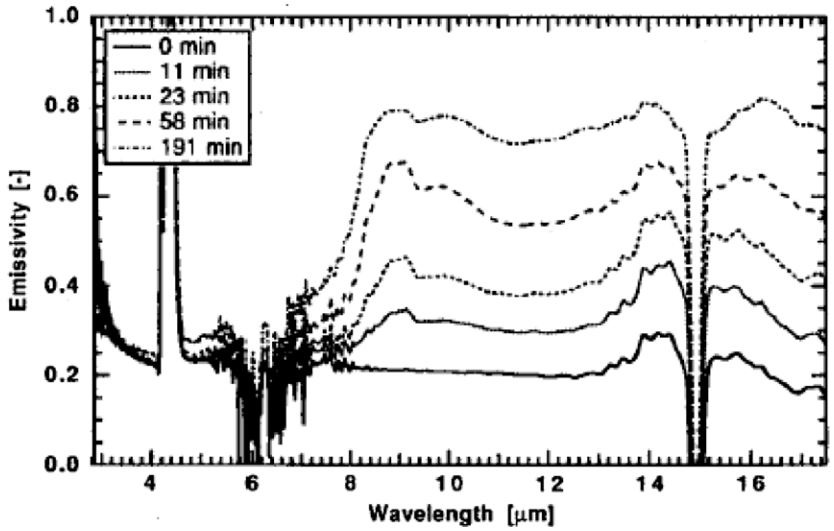

Fig. 4. Spectral emittance of ash deposit vs. time of deposit growth [9].

pletely clean tubes. It was concluded that the measured emittances strongly depend upon wavelength as indicated the influence of physical properties and chemical composition of deposits. At wavelengths above 7 μm, emittance reaches a constant value caused by thickening of the deposit and increase of size of its particles.

At shorter wavelengths the deposit ceases to be opaque and the emittance (now it is the "apparent" emittance) is dependent upon the properties of (i.e. conditions at) the metal surface of the tube at which the deposit was formed, and of the particles. Also, the measurement results reveal the influence of triatomic molecules of carbon dioxide (CO_2) and water (H_2O) that strongly absorb the radiation: CO_2 – in spectral bands 4.2–4.7 μm and 14.4–15.2 μm, and H_2O – in spectral bands 2.9–3.0 μm and 5.5–7.5 μm.

Theoretical predictions of spectral emitance of ash deposits, as a function of particle size and chemical composition, have been also made in this work (Fig. 5) and these results were compared with measured data. Predicted trends of spectral emittance vs. particle size comply with the experimentally obtained results in a great extent.

The authors of article [11] have presented their own experimental and analytical results showing the influence that the dependent effects (scattering and absorption are called dependent effects if these phenomena of a particle in a medium are affected by the neighbouring particles) exert upon the determination of the ash deposit emittance. In that paper a model is outlined – for determining the spectral emittance (directional, normal and hemispherical) of certain semi-transparent and opaque deposits – that deliberately does not consider the dependent effects. The predictions illustrate the influence that particle size and chemical composition exert upon emittance of coal ash deposits.

While both the measured and the predicted values of total hemispherical emittance of the deposits are apart by approximately the same value, attributed to the chemical composition, the difference between the measured total emittance values and – the predicted values (by the virtue of "non-dependent theory") was pronounced (Fig. 6) especially for the more transparent materials. Apparently, in these diagrams there is no "hysteresis" characteristic for the experiments performed when doing research on these phenomena (e.g. in [1,9,16]). This is because, for simplicity,

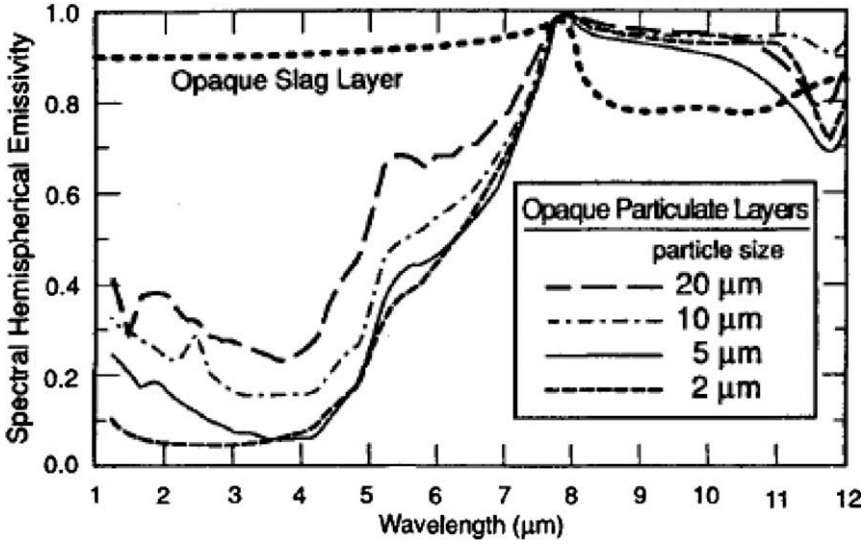

Fig. 5. Prediction of deposit spectral emittance vs. particle size [9].

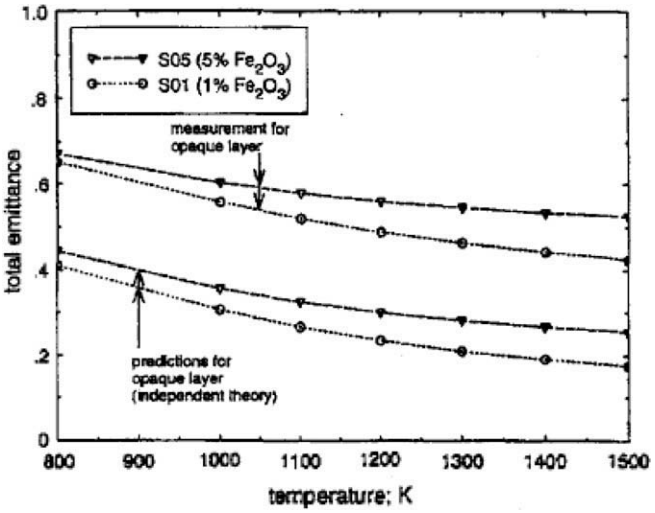

Fig. 6. Measured/predicted emittance of opaque granular ash deposit [11].

the authors had considered the deposit in its already sintered and fused state – realistic for hotter furnaces.

Another paper [12] by the same group of authors includes a review of the most frequently utilised experimental methods for determining the total emittance of powdered deposits. The most of authors place the specimen in a vessel that is heated from below and the top surface is monitored for the radiation intensity measurement. The emittance is determined by comparing this intensity with blackbody radiation intensity at the same temperature. The author of [12] has described the computations used to quantitatively determine the difference of emittance of isothermal and non-isothermal deposits. A 1-D model was developed for that purpose and a 5 mm thick deposit was considered to be divided into 1000 layers. The temperature gradient through the deposit was assumed linear, and the temperature within each layer – constant. The 1.2–12 μm spectrum was subdivided into 55 intervals 0.2 μm wide within which the radiation properties were considered constant and different. Also, the hemisphere – the layer is radiating heat into – was divided in 16 directions (ordinates) with corresponding weight (mass) factors. Values of the real refraction and absorption index are of three different ash deposits.

That model has enabled the computation of minimal sample layer thickness that still ensures opacity and – enabled predicting the emittance. It is shown that the emittance can be significantly different for isothermal and non-isothermal deposits in the case of presence of a large temperature gradient through the layer and/or larger particles.

Impact of optical constants and particle size upon radiation characteristics and furnace heat transfer rate was analyzed in a subsequent article [13] by the same research group. In the majority of computations, authors utilized the value of the spectral complex refraction index from the paper [8] that was obtained experimentally for four artificial deposits with different content of ferric oxide (Fe_2O_3) ranging from 0.85% to 16.53% (SA01, SA05, SA10 & SD20, respectively). The analysis had encompassed 2 different particle size distributions (mean size/diameter 3.25 μm and 15 μm) and assumptions on: spherical form of particles, equal chemical composition (equal complex refraction index) and uniquely non-dependent and multiple scattering.

The authors have observed that the impact of the real refraction index, $n\lambda$, upon the spectral emittance (for fine particles) is felt in the whole wavelength range (Fig. 7) and that it is pronounced if the deposit is a better absorber. For a sample of a material that is a weak absorber, the influence of real index is significant only at wavelengths above 5 μm. Same trend is observed with coarser particles, however this effect is less pronounced. As well, the spectral emittance is somewhat larger for coarser particles.

Considering the absorption index, $k\lambda$, all the effects are prominent at wavelengths below 5 μm. In this (near infrared) part of the spectrum, iron has a strong impact upon the spectral absorption index, and thus upon the spectral hemispherical emittance (Fig. 8) too. Particle size affects the emittance strongly, as well, but only at wavelengths below 8 μm. In this spectral range, coarser deposits (composed of larger particles) have larger spectral emittance than the finer deposits (composed of smaller particles).

Considering the outlined research, the following point deserves to be focused onto. Thermal radiation properties of ash deposits are strongly temperature dependent. Spectral behavior of ash deposit is the main cause of the strong temperature dependence of total emittance. Data on emittance of Serbian (and other as well) lignites and their ashes are scarce. These data are considered to find themselves among the main parameters in steam boiler design (in thermal power plants and fruit and vegetables drying), so the present authors undertook research on thermal radiation properties of Serbian coal ash.

Spectral normal emittance (in 2.5–25 μm range) and total normal emittance were measured on 4 kinds of ash layers of a mm order thickness, at 560–1460–560 K in heating and cooling. Their dependence on λ and T, and upon ash sintering and fusion, was studied. The authors propose, and explain by an example, correlating the experimentally obtained emittance spectra by a continuous function that defines the dependence of ε on λ and T. This may greatly simplify the practical application of the experimentally determined emittances in the thermal design of existing and new steam boiler furnaces.

2. Experimental procedure

2.1. Materials of specimens

Materials of the specimens are broken pieces of flying ash deposits on a boiler furnace heat exchange surfaces of a power plant in Serbia, where pulverized lignite is combusted. These pieces were sampled at four positions along the furnace height as it is shown in Table 1. The materials are inorganic compounds that are solidified like rocks with the inhomogeneities of an order of mm. The pieces were powdered manually and – layers of the sampled pieces are prepared. Average properties of the powdered ash layers were investigated by conducting the experiments, specified later in the text.

Table 1 shows the specification of ash specimens, where ρ_p is the heaping mass density. Table 2 presents the chemical composition of the same four ash specimens.

2.2. Specimen layers

Fig. 9 presents a schematic diagram of the experimental set-up. Powder of an ash specimen is set in a vessel /1/ of stainless steel JIS-SUS304 (1, 3 or 5 mm deep) to form a specimen layer /2/. Surfaces of the vessels are oxidized enough in advance so the surface state would not change during the measurement. A K-type thermocouple was welded on the rear surface of the vessel for temperature control of the specimen layer.

Temperature of the specimen layer was measured by a K-thermocouple /3/ of 100 μm in diameter. The hot-junction of the thermocouple is set at a position of 0–0.5 mm depth by lightly pressing it into the layer. The specimen layer is radiation-heated from the back by four silicon carbide rod heaters /4/. A water-cooled copper radiation shield /5/ has been located at the very surroundings of the powdered ash deposit specimen surface, so

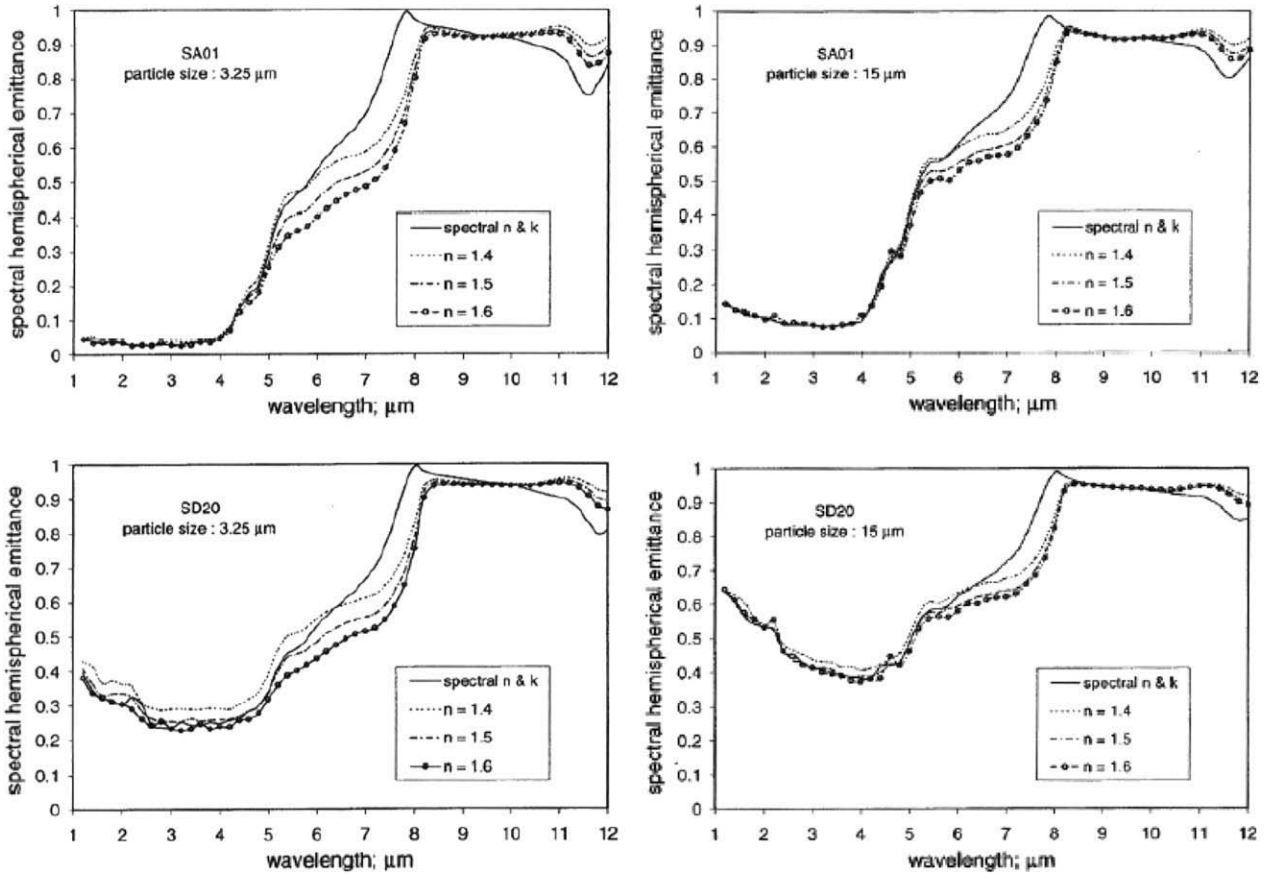

Fig. 7. Influence of index "n" on spectral emittance of opaque granular deposit [13].

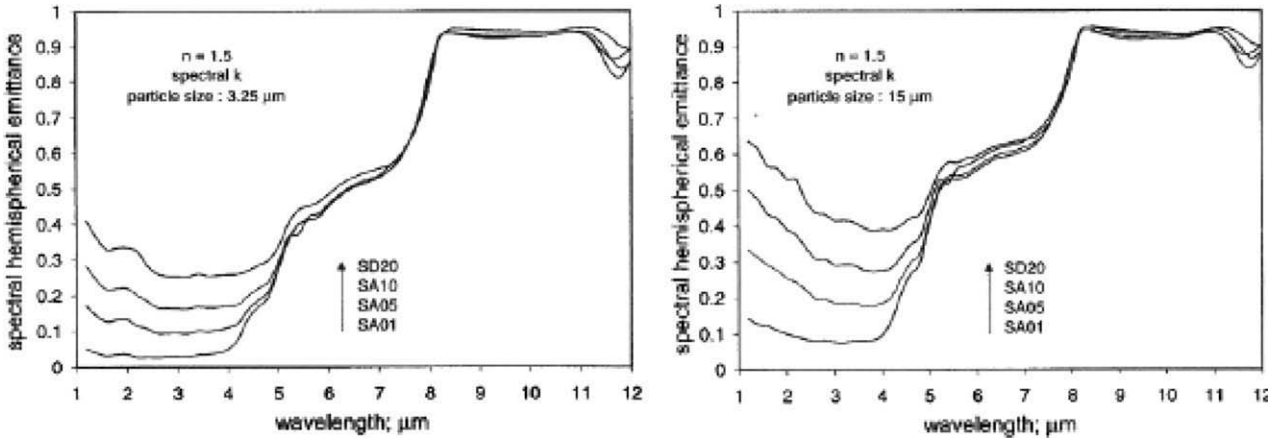

Fig. 8. Absorption index vs. spectral emittance of opaque granular ash deposit [13].

that the radiation emitted by hot surroundings of the specimen is not multiply reflected and does not reach and affect the optical measuring system.

The specimen layer is heated up to ≈560 K by heating rate of 2 K/min, common for similar experiments, and optical measurement (see Section 2.3) is made. Heating is continued at the same rate and at every 100 K up to ≈1460 K similar optical measurement is repeated. This value of maximum temperature was chosen because, it is common [1,6,7] that ash of similar chemical composition and granulation is yet sintered and fused (molten) – before reaching it. (This coincides with observations on cooled-down specimens.) At reaching the maximum temperature, the specimen is cooled down with the cooling rate of 2 K/min and, at every 100 K down to ≈560 K, optical measurement is repeated.

2.3. Optical measurement

Fig. 10 shows (in axonometry) the spatial position of the experimental set-up, during the optical measurement of: (a) spectral emissive power; and (b) total emissive power. At every 100 K, the movable mirror is being displaced out of the observation area of the spectrophotometer /7/, which accepts the specimen radiation flux within the solid angle defined by a zenith angle of ±10°, and the (a) measurement is done; then the movable mirror is slid-

Table 1
Specification of powdered ash deposit specimens.

	Height in furnace	Structure	Color		ρ_p (kg/m^3)
			Bulk	Powder	
1	10 m, inclined wall	s-granular i-layer	Brown Dark red	Pink	1378
2	30 m, rear wall	s-granular i-layer	Brown Black	Brown	1469
3	46 m, super heater	s-layer i-layer	Violet Dark red	Pink	898
4	10 m, inclined wall	s-granular i-layer	Violet Dark red	Brick red	1199

(s, specimen surface; i, interior part of the specimen).

Table 2
Chemical composition of ash specimens (wt.%).

	No.1	No.2	No.3	No.4
$CaSO_4$	48.2	25.9	53.4	42.5
CaO	4.7	18.9	4.5	9.9
Al_2O_3	3.1	3.4	2.6	4.2
FeO	29.4	35.3	25.7	28.4
SiO_2	7.4	9.5	7.4	8.3
Others	7.2	7.0	6.4	6.7

ed above the specimen to the position for (b) measurement, and it is done by redirecting the same radiation flux to the total radiation fluxmeter /8/.

Emittance of specimen ash layers is measured by a comparison method in which the radiation emitted from the specimen surface is compared with that emitted from the reference blackbody /9/. The spectrophotometer, that is being utilized for the infrared spectral measurement, is Fourier transformation type (Shimadzu Co., FTIR-4200, [14]), which monitors the spectrum of 1868 wavelength points in the region of wavelengths $\lambda = 2.5–25$ μm, where more than 95% and 75% of radiation energy of the blackbody at temperatures of 560 K and 1460 K are covered, respectively. Spectral resolution of the FTIR spectrophotometer is 2 cm^{-1} at $\lambda = 12.3$ μm, which is rather too fine for the thermal engineering research. Total radiation fluxmeter for the total emittance measurement is a modified radiation type pyrometer (Minolta Co., 505S, [15]), which senses the infrared radiation by a thermoelectric detector via two non-coated aluminum mirrors and a KRS-5 window. Spectral absorption characteristics of the mirrors and the window are checked to be gray enough over $\lambda = 1–40$ μm region, but that of the detector is not assured.

The reference black body is a cylinder – type one. Temperatures of the interior surface of the blackbody are measured by using a radiation pyrometer that was calibrated using the standard black-

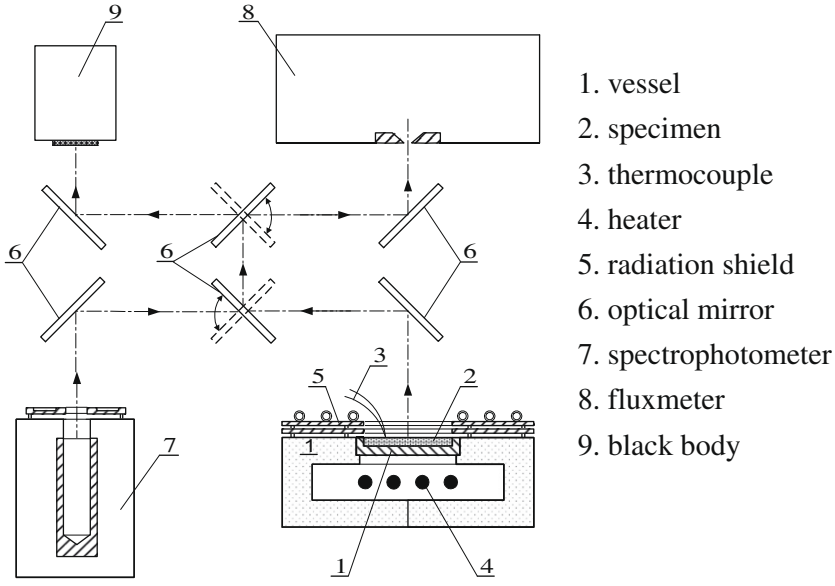

Fig. 9. Schematic diagram of the experimental test set-up.

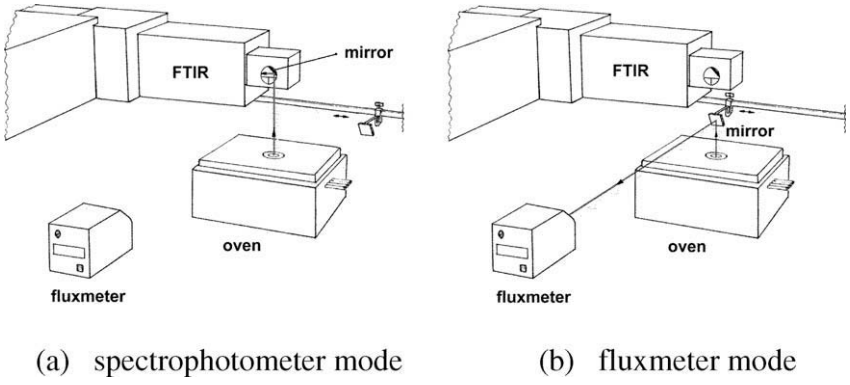

Fig. 10. Axonometric image of the set-up for optical measurement.

bodies at the National Research Laboratory of Metrology, Tokyo, Japan. Temperature of the reference blackbody was controlled by utilizing the measured values of a thermocouple installed within the black body.

The intensity $v_B(\lambda_i,T_{Bj})$ of blackbody radiation at temperature T_{Bj} measured by the spectrophotometer at each wavelength λ_i is described by the relation outlined in [17]

$$v_B(\lambda_i,T_{Bj}) = \frac{A(\lambda_i)}{e^{\frac{c_2}{\lambda_i T_{Bj}}}-1} + \frac{B(\lambda_i)}{e^{\frac{c_2}{\lambda_i T_{Broomj}}}-1} \quad (1)$$

where the second term does compensate the influence of ambient radiation at the room temperature. $A(\lambda_i)$ and $B(\lambda_i)$ are the measuring system constants that depend upon the wavelength, and T_{Broomj} is the room temperature at the time of optical measurement at the blackbody temperature T_{Bj}. Intensity $v_B(\lambda_i,T_{Bj})$ at each wavelength λ_i is measured in advance at several temperatures T_{Bj} to determine the constants $A(\lambda_i)$ and $B(\lambda_i)$. Then, emittance of the specimen at temperature T_S, which can be set roughly, is calculated [17]

$$\varepsilon_N(\lambda_i,T_S) = \left[v_S(\lambda_i,T_S) - \frac{B(\lambda_i)}{e^{\frac{c_2}{\lambda_i T_{Sroom}}}-1}\right] : \frac{A(\lambda_i)}{e^{\frac{c_2}{\lambda_i T_S}}-1} \quad (2)$$

where $v_S(\lambda_i,T_S)$ is the measured radiation intensity of the specimen layer and T_{Sroom} is room temperature at the time of the optical measurement. The measurement at each temperature is finished within several minutes. Temperatures of the blackbody, specimen and room do not change significantly during this period.

Total intensity $v_B^{total}(T_{Bj})$ measured by the total fluxmeter is described as in [17]

$$v_B^{total}(T_{Bj}) = A^{total}T_{Bj}^4 + B^{total}T_{Broomj}^4 \quad (3)$$

where A^{total} and B^{total} are constants of the total emittance measurement system. Intensity $v_B^{total}(T_{Bj})$ is measured in advance at several temperatures T_{Bj} to determine the constants A^{total} and B^{total}. Total emittance of the specimen at T_S can be computed as in [17] by

$$\varepsilon_N^{total}(T_S) = \left\{v_S^{total}(T_S) - B^{total}T_{Sroom}^4\right\} \Big/ \left(A^{total}T_S^4\right) \quad (4)$$

where $v_S^{total}(T_S)$ is the measured total radiation intensity of the specimen layer, and T_{Sroom} is the room temperature at the time of the optical measurement.

2.4. Experimental error

Total normal emittance and spectral normal emittance were measured by an open measurement system so that reflection of the irradiation from the surroundings of the specimen was not included into the emission of the specimen, as it is in furnaces. The specimen was heated from the back. Since thermal conductivity of the inorganic materials is not so high as that of the metals, temperature distribution is formed in the specimen layer, which lifts the following problem. Thermocouple for measuring the surface temperature was not set at certain point in depth direction, and thermal contact with the powdered specimen was not ideal.

Thence, it was not an obviously solvable task to estimate the error of emittance determination caused by the error of the temperature measurement. Therefore, based on several repeated experiments with the specimen No.1 (5 mm) at $T = 1000$ K the standard deviation was computed by the commonly used relation:

$$SD = \sqrt{\frac{(\varepsilon_1-\bar{\varepsilon})^2 + (\varepsilon_2-\bar{\varepsilon})^2 + \cdots + (\varepsilon_n-\bar{\varepsilon})^2}{n-1}} \cdot \frac{100\%}{\bar{\varepsilon}} \quad (5)$$

where: ε_1, ε_2, ..., ε_n– experimentally determined emittances, $\bar{\varepsilon}$ – arithmetic mean of these emittances, n – number of repeated experiments.

Standard deviation of the measured ε_N values from the average value lies within ±4.2 and ±2.2% at $\lambda = 3.75$ and 12.5 μm, respectively. On the other hand, standard deviation of the measured ε_N^{total} values from the average value is ±4.7%.

3. Results and discussion

3.1. Total emittance of ash layers

Temperature dependence of total (hemispherical) emittance of tested ash layers was analyzed. All four specimens (No.1–4 of $t = 5$ mm) were tested at 560–1460–560 K (heating + cooling, Section 2.3). Two types of total emittance were compared: ε_N^{total}, measured by the total fluxmeter, was compared to $\varepsilon_N^{2.5-25\mu m}$, computed from spectra of emittance ε_N (measured over $\lambda = 2.5$–25 μm in the present experiment) as in [17]:

$$\varepsilon_N^{2.5-25\mu m} = \frac{\int_{2.5\mu m}^{25\mu m} \varepsilon_N(\lambda,T_S)\cdot v_B(\lambda,T_S)d\lambda}{\int_{2.5\mu m}^{25\mu m} v_B(\lambda,T_S)d\lambda} \quad (6)$$

This integral-differential equation is solved as sum-difference equation, Eq. (7), by approximating integrals w. sums, by using "trapezoidal rule" of numerical integration:

$$\varepsilon_N^{2.5-25\mu m} = \frac{\sum_{i=1}^{1867} \frac{\varepsilon_N(\lambda_{i+1},T_S)\cdot v_B(\lambda_{i+1},T_S) + \varepsilon_N(\lambda_i,T_S)\cdot v_B(\lambda_i,T_S)}{2}\cdot(\lambda_{i+1}-\lambda_i)}{\sum_{i=1}^{1867} \frac{v_B(\lambda_{i+1},T_S)+v_B(\lambda_i,T_S)}{2}\cdot(\lambda_{i+1}-\lambda_i)} \quad (7)$$

Since more than >95% (75%) of Planck black-body emission at 560 K (1460 K) lies within this wavelength region, total emittances $\varepsilon_N^{2.5-25\mu m}$ and ε_N^{total} are comparable. Temperature dependences of both types of total emittance (of Specimen No.1) are shown in Fig. 11.

It is obvious that the temperature dependences of $\varepsilon_N^{2.5-25\mu m}$ and ε_N^{total} comply with each other. The same conclusion holds for the three other Specimens (No.2–4). This fact does indeed mutually confirm (i.e. verifies) the validity of both simultaneously conducted measurements: (a) using FTIR spectrophotometer and (b) using total radiation fluxmeter. Also, comparison of Figs. 11 and 1, i.e data from the present experiment and data of other authors, that obviously do comply well, additionally confirms this validity.

Fig. 12 presents the four plots (for – all four specimens) of total emittance of ash deposits vs. temperature, for the complete course of the present experiment, in processes of specimen heating and cooling, that begins after reaching the maximum temperature of the process (Specimens No.1–4, at $T = 560$–1460–560 K). As it is easily observed, curves comply qualitatively and quantitatively, among themselves, as well as with characteristic results of other

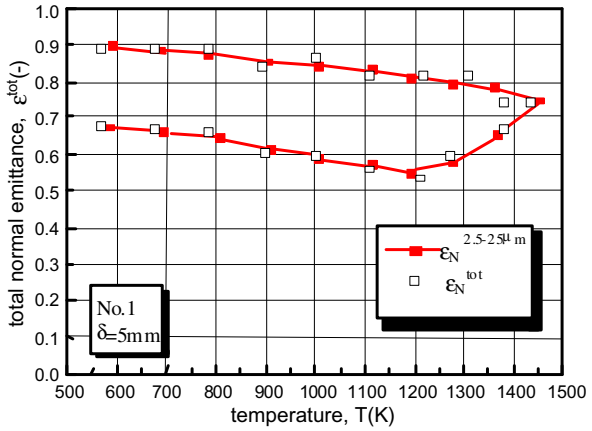

Fig. 11. Temperature dependence of total emittance of an ash layer.

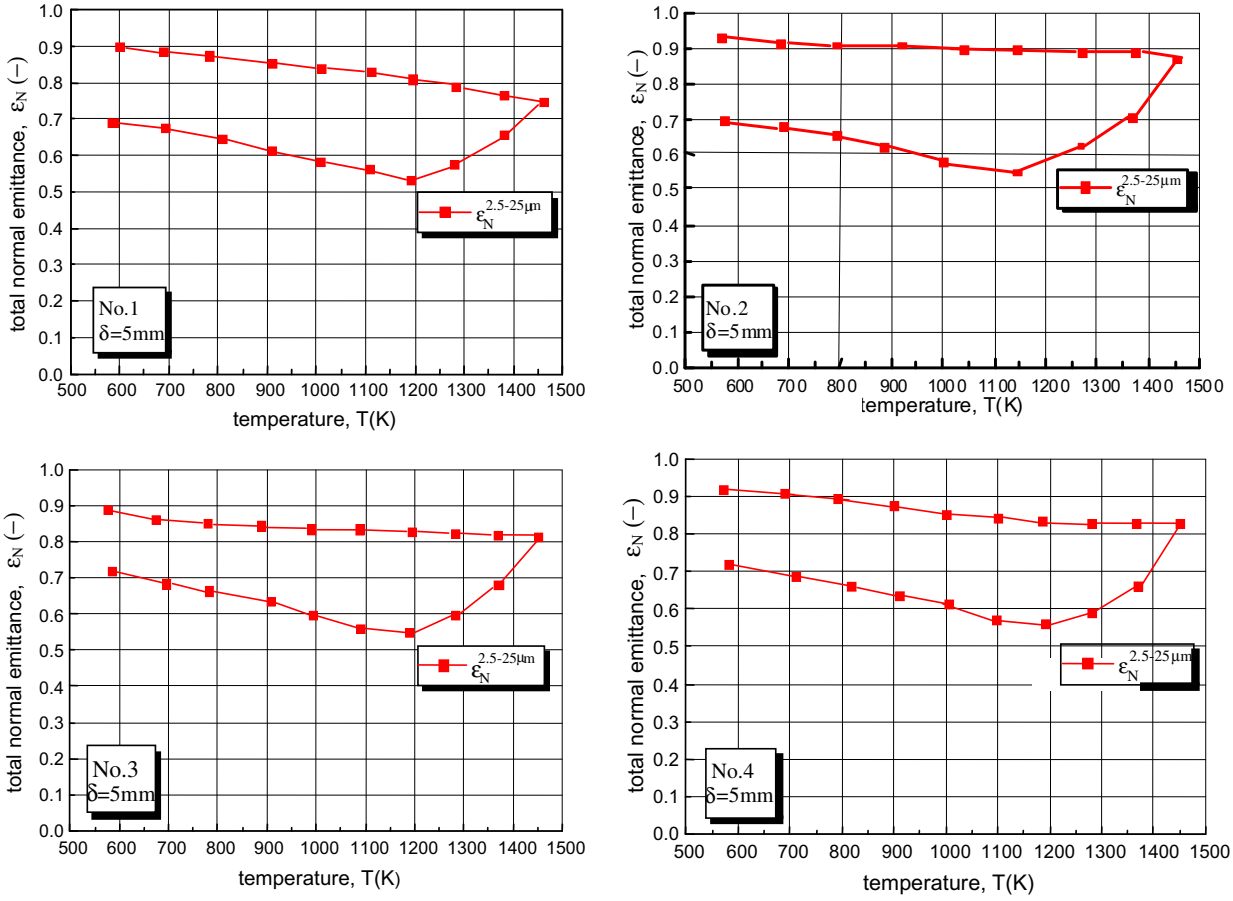

Fig. 12. Total emittance of ash deposit layers vs. temperature in heating and cooling.

authors [6,7,9,11,16]. All curves have a common "ship like" form, that is the general consequence of the "hysteresis". This clearly illustrates a permanent change (increase) of emittance due to two irreversible phenomena: sintering and fusion.

3.2. Emission spectra of ash layers

Fig. 13 shows the spectra of emissive power of thermal radiation flux of an ash deposit layer, within the narrow solid angle defined by a zenith angle of ±10°. The spectra shown have been measured during the heating process in the 580–1460 K temperature interval, and represent an example of raw measurement data. Similar spectra have been gathered during the cooling part of the complete process, i.e. in the 1460–560 K interval. Both (heating and cooling) spectra were measured in accordance with the methodology set in Section 2.3, on Specimen No.1 (5 mm thick).

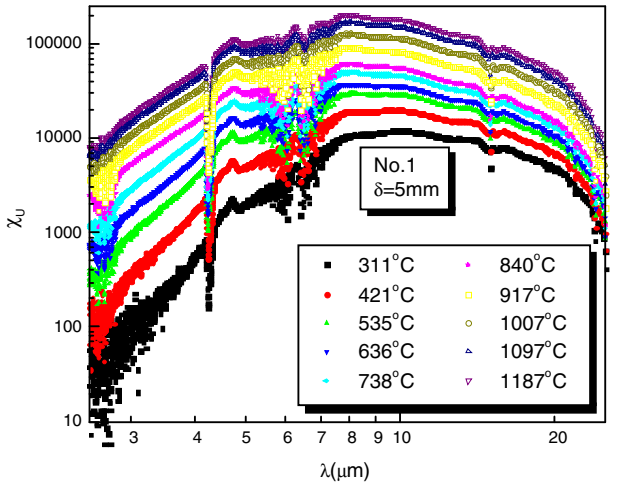

Fig. 13. IR emissive power spectra of an ash layer – heating part of the process.

For clarity of the graphical representation, a common data reduction method has been used. The arithmetic mean of the emissive power values was determined, for each of the 1868 wavelength values, out of eleven (five – at left, one – central and five – at right) neighboring data points. After this data processing has been performed, the plot consists only of every 11th so-determined consecutive values. In that manner, for a specimen at a certain temperature, only 187 data points are plotted instead of the multitude of 1868 data that are measured in the present experiments, by the FTIR spectrophotometer.

In the plot, one clearly observes the influence of triatomic gases, present in the air above the heated specimen, that have the ability to absorb the radiation in certain intervals of wavelength (absorption bands) in the infrared spectral region. The carbon-dioxide and water-vapor absorption bands are pronounced in the $\lambda = 2.6$–2.7 μm range, absorption by only CO_2 in the bands about $\lambda = 4.3$ μm, and about $\lambda = 15$ μm, and absorption by only H_2O in the band about $\lambda = 6.3$ μm. Absorption by CO_2 exerts a most critical distortive effect on the measurement results in the $\lambda = 4$–5 μm region, with high absorption peaks.

3.3. Radiation transmission through ash layers

In the specimen system of the present experiment, the temperature distribution is formed in the depth direction. Since temperature dependence of emittance is not strong, emittance does not

vary very significantly in the depth direction. But, if a powdered ash deposit specimen layer were semi-transparent for the infrared radiation, radiation emitted at the part below the surface, or at the specimen vessel, could yet be measured, and the measured emittance ε_N, which is thus being normalized by the surface temperature, would remain to be an apparent emittance ε_{Nap}. The apparent value would be higher than the true emittance and therefore not representative of the genuine ash deposit.

Dependence of measured spectral emittances, at a low emittance wavelength and at a high emittance wavelength, i.e. $\lambda = 3.75$ and 12.5 μm, of powderd ash deposit layers on their thickness is shown in Fig. 14. The data presented here are those obtained from the tests on Specimens No.1–4 of thickness $t = 1$–5 mm at ≈1000 K in heating and cooling processes. It is obvious that the emittance ε_N does not depend substantially on thickness t of the specimen layer in each specimen and at the shorter and longer wavelengths (of $\lambda = 3.75$ and 12.5 μm). It is concluded that even the layers of thickness $t = 1$ mm are opaque enough. Measured emittances ε_N of the layers are considered to be the true emittances, that are duly representative property values of the considered ash deposit material.

3.4. Emittance spectra of ash layers

Spectral emittances of the four ash deposit layers, in the direction perpendicular to specimen surface (within the solid angle defined by a zenith angle of ±10°), during their heating in 560–1460 K range, in the course of a complete experiment (560–1460–560 K) are shown in Fig. 15 – left, for the four tested ash deposit specimens (No.1–4) of equal thickness ($t = 5$ mm). These values are determined by using the formulae (1) and (2) i.e. by following the methodological approach that is described in Section 2.3.

One can observe that emittance (at a constant temperature) continually increases with the wavelength in each spectrum. The

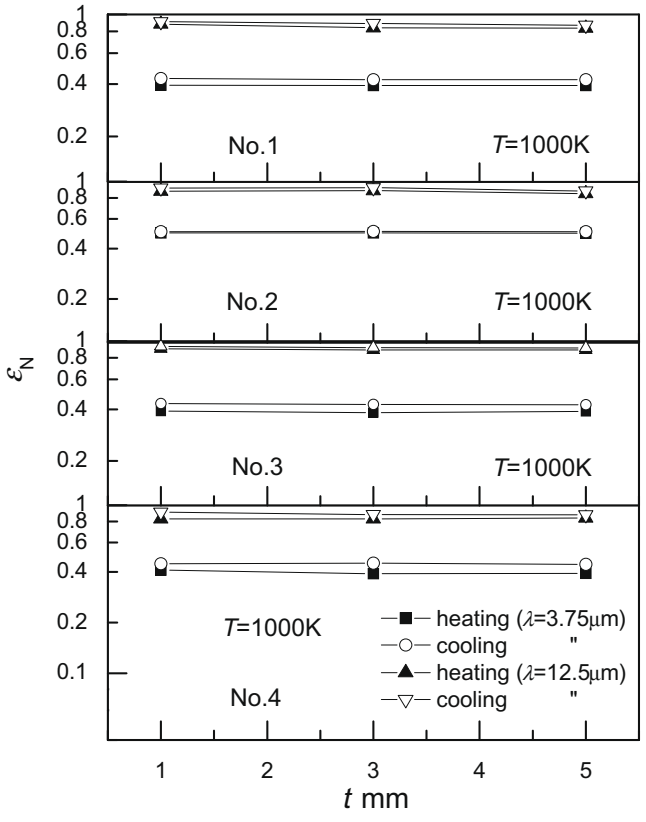

Fig. 14. Spectral emittance ($\lambda = 3.75$ and 12.5 μm) vs. thickness of ash layers.

increase is steep in the central part of each spectrum ($\lambda = 4$–7 μm). To the left and to the right from this interval, the emittance is practically constant, i.e. it is not sensitive to the change in wavelength. However, for λ lower than 4 μm – increase of emittance with temperature is noticeable, while in 4–7 μm range the same dependence weakens with wavelength. Also, at values higher than 7 μm – isothermal lines of spectral emittance of ash deposits practically co-incide.

Fig. 15 – left presents the ash deposit emittance spectra. Fig. 15 – right shows the curve fits of these experimental spectra, as it is described in detail in Section 4. Here we will just state that we propose the following function to correlate the empirical points,

$$\varepsilon_H(\lambda) \cong \varepsilon_N(\lambda) = \frac{\varepsilon_{\min} + \varepsilon_{\max}\left(\frac{\lambda}{\lambda_m}\right)^p}{1 + \left(\frac{\lambda}{\lambda_m}\right)^p} \tag{8}$$

where: $\varepsilon_{\min}$, $\varepsilon_{\max}$ are – horizontal asymptotes of the fitting line (curve fit) i.e. emittances for $\lambda \to 0$ and $\lambda \to \infty$. Also, λ_m and p are, respectively: abscissa of the mid-point of the slope and – the slope power (exponent). Each plot contains 10 curve fits for – 10 fixed measuring temperatures. The spectra of ash deposit emittance (and fits) for cooling of the Specimens No.1–4 (Fig. 16), are of the same form like – during heating. The emittance increases too – with temperature in the $\lambda = 2.5$–4 μm range, however all lines (for constant temperatures) are noticeably higher. This "hysteresis" tendency is a direct consequence of the irreversible physical and chemical changes occurring during the processes of sintering and fusion (melting) of ash deposits at temperatures above 1200 K.

4. Correlating data for engineering application

To solve the radiation heat transfer in a boiler accurately, under sharp temperature distribution, spectral analysis is recommended today [16–18] as well as it was two decades ago [19]. That is so because using data of emittance spectra of ash layers is more adequate than the traditional total analysis, using those of total emittance. Of course, emittance used in classical radiation energy exchange calculations, using configuration factors, is the hemispherical emittance ε_H, that is not identical to the normal emittance ε_N of the present measurement. But, as mentioned earlier, directional characteristics of the emittance are weak [6], and thence the values of ε_N are considered close enough to those of ε_H. This is a vital issue since, clearly, it is much simpler (and cheaper) to measure the emissive power in normal direction than – into hemisphere.

For an actual engineering application, it is desirable that ε_H spectrum is in a form of a continuous function of radiation wavelength λ and temperature T. This contributes to the extrapolation of the wavelength region and – also to the convenience of the numerical computation. We proposed the function (8) to correlate the experimentally determined points. The empirical curves, shown in Fig. 15 – left and 16 – left, were treated by a best-fit method – to solve for the parameters. Tables 3–6 present data and the result of the performed research – the obtained temperature dependent correlations: $\varepsilon_{min}(T)$, $\varepsilon_{max}(T)$ and $p(T)$ for the 4 tested specimen layers (heating + cooling) that are usable in the thermal design of the very furnace where the samples are taken from but as well as in the thermal design of similar furnaces combusting the same type of coal.

Fig. 15 – right and 16 – right, are curve fits obtained by fitting the measurement results by the function of simple visual and analytical form, as defined by Eq. (8). It presents the chosen functional dependence of spectral emittance upon wavelength and temperature: $\varepsilon_H \approx \varepsilon_N(\lambda, T)$. The same figures contain curves fitted – for each temperature separately – during specimen heating and cooling. The lines

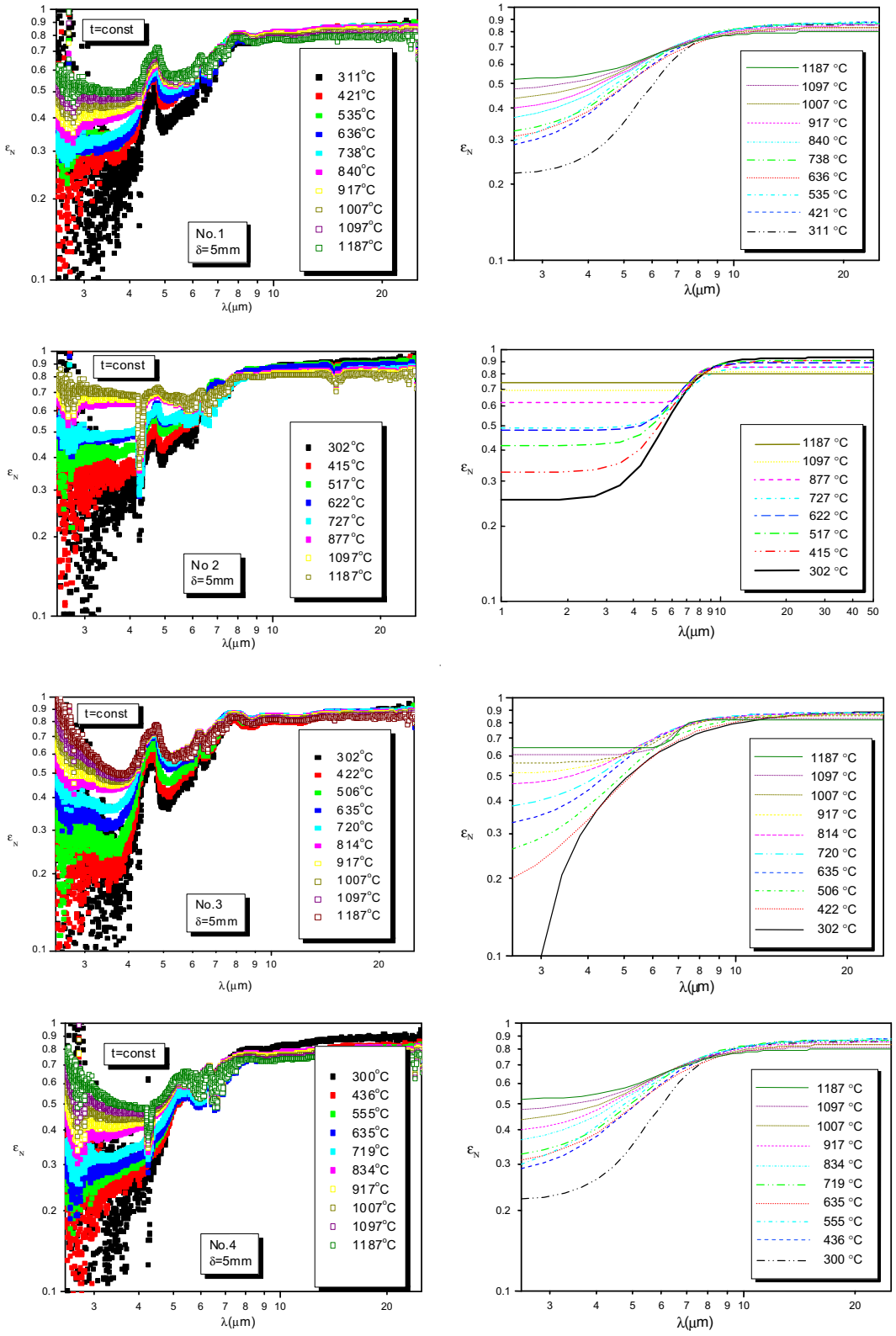

Fig. 15. Spectra of ash deposit emittance in heating mode (left = experiment; right = fit).

are extrapolated beyond the wavelength region of the experiment. However, in the far–infrared region up to several ten μm, in wavelength, outside the experimental region, various lattice vibration modes in the complex inorganic crystals in the ash are distributed all over the region, and strong absorption with high emittance is preserved here. In the near-infrared region outside the present experiment, the short wavelength tail of the Planckian energy distribution to be multiplied with the emittance is low enough,

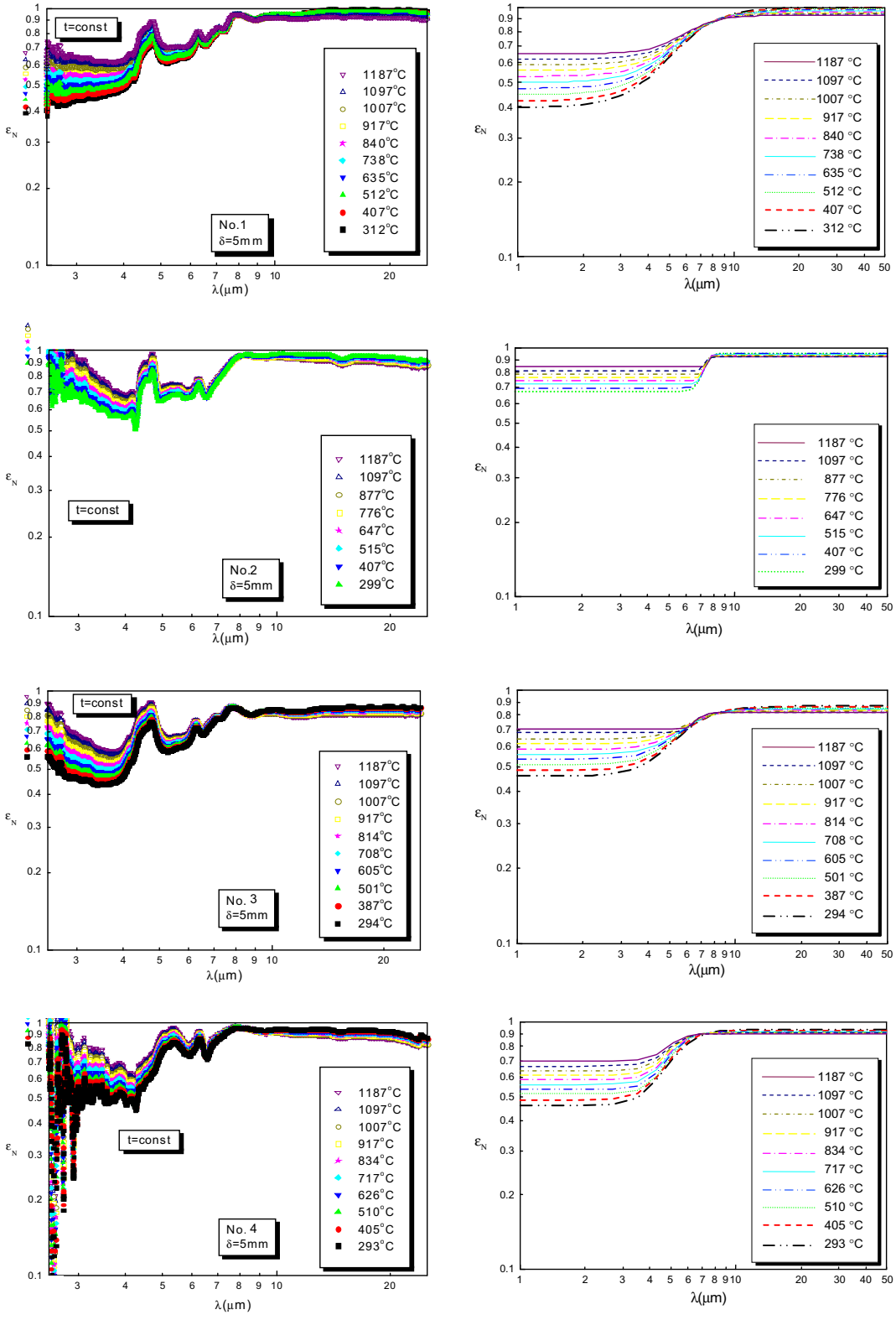

Fig. 16. Spectra of ash deposit emittance in cooling mode (left = experiment; right = fit).

and therefore the crude assumption of the emittance in this region, made as the simplest solution under these circumstances, does not exert any significant effect on the computed energy flux.

Tables 3–6 contain the values of: ε_{min}, ε_{max}, λ_m and p – for each specimen in heating and cooling – for each temperature the measurements were done at. In the bottom of each table, the recommended formulae of temperature dependent functions: $\varepsilon_{min}(T)$, $\varepsilon_{max}(T)$ and $p(T)$ are shown. Parameter λ_m is (obviously) not too sensitive to temperature changes, thus, its mean value can be used, for simplicity. A rough analysis of the data suggests that: (A) the empirical correlations for $\varepsilon_{min}(T)$, $\varepsilon_{max}(T)$, $p(T)$ and λ_m – related to deposit heating – can be used only for furnace

Table 3
Parameters: $\varepsilon_{min}(T)$, $\varepsilon_{max}(T)$, $p(T)$ and λ_m, of the function $\varepsilon_H(\lambda,T)$ for Sample 1.

Sample 1									
Heating					Cooling				
T/K	ε_{min}	ε_{max}	λ_m/μm	p	T/K	ε_{min}	ε_{max}	λ_m/μm	p
584	0.20208	0.86962	6.08715	4.39428	1461	0.65927	0.92718	6.04162	5.33628
694	0.23886	0.84221	5.75570	4.14474	1371	0.62001	0.93431	5.93151	4.99022
808	0.28159	0.83875	5.76056	4.40036	1280	0.58890	0.94174	5.84969	4.73292
909	0.29111	0.83664	5.74377	4.12819	1189	0.55854	0.94944	5.78825	4.52931
1011	0.26867	0.87498	5.45810	3.75120	1108	0.52900	0.95739	5.74238	4.36285
1113	0.34480	0.86927	5.66197	3.85477	1009	0.50039	0.96554	5.70883	4.22428
1190	0.37808	0.85226	5.57212	3.55987	908	0.47278	0.97387	5.68543	4.10777
1279	0.41384	0.83618	5.45762	3.20396	785	0.44624	0.98235	5.67057	4.00924
1370	0.45034	0.82183	5.28205	2.74412	680	0.42081	0.99096	5.66307	3.92568
1461	0.48014	0.81161	4.89194	2.10085	565	0.39652	0.99966	5.66197	3.85477
$\varepsilon_{min} = -0.95345 + 0.18209 \ln T$ $\varepsilon_{max} = 0.76141 + 0.01395 \ln T$ $\lambda_m = 5.74454$ $p = 10.10669 - 0.8913 \ln T$					$\varepsilon_{min} = 0.28924 + 0.01473 \ln (T - 565)$ $\varepsilon_{max} = 1.77634 - 0.12915 \ln T$ $\lambda_m = 5.3425$ $p = 4.20326 + 0.05246 \ln (T - 565)$				

Table 4
Parameters: $\varepsilon_{min}(T)$, $\varepsilon_{max}(T)$, $p(T)$ and λ_m, of the function $\varepsilon_H(\lambda,T)$ for Sample 2.

Sample 2									
Heating					Cooling				
T/K	ε_{min}	ε_{max}	λ_m/μm	p	T/K	ε_{min}	ε_{max}	λ_m/μm	p
575	0.25373	0.93048	6.18377	5.04634	1459	0.84152	0.92147	7.45336	122.86190
688	0.32528	0.90441	6.17944	5.14109	1369	0.81489	0.92600	7.40928	86.31251
790	0.41750	0.90651	6.34646	6.09828	1151	0.78909	0.93061	7.36751	66.69479
895	0.47834	0.89100	6.53634	6.84490	1049	0.76408	0.93530	7.32872	54.44231
1000	0.49071	0.85639	6.88179	6.43806	920	0.73984	0.94012	7.29286	45.64349
1150	0.61686	0.85572	7.22129	15.72937	788	0.71630	0.94512	7.25917	38.53803
1371	0.69248	0.82238	7.55900	39.56941	680	0.69336	0.95040	7.22606	32.25683
1459	0.74296	0.80514	7.69630	100.57088	572	0.67084	0.95612	7.19054	26.35178
$\varepsilon_{min} = -2.95693 + 0.50416 \ln T$ $\varepsilon_{max} = 1.64314 - 0.11198 \ln T$ $\lambda_m = 6.55818$ $p = -238.44449 + 32.0406 \ln (T + 1317)$					$\varepsilon_{min} = 1.17802 - 0.08626 \ln (T - 412.75833)$ $\varepsilon_{max} = 6.10311 - 0.65156 \ln (T - 20233.123)$ $\lambda_m = 7.22836$ $p = 203.08212 - 26.46075 \ln T$				

Table 5
Parameters: $\varepsilon_{min}(T)$, $\varepsilon_{max}(T)$, $p(T)$ and λ_m, of the function $\varepsilon_H(\lambda,T)$ for Sample 3.

Sample 3									
Heating					Cooling				
T/K	ε_{min}	ε_{max}	λ_m/μm	p	T/K	ε_{min}	ε_{max}	λ_m/μm	p
575	−0.0306	0.90156	4.8804	3.11763	1461	0.70493	0.81779	6.6835	28.9421
695	0.17058	0.86521	5.3341	3.94431	1370	0.68105	0.82139	6.5750	22.1733
779	0.24027	0.86664	5.3218	4.31238	1281	0.64452	0.82787	6.0496	7.05926
908	0.31175	0.87738	5.1907	4.66818	1191	0.61598	0.83265	5.9028	6.46196
993	0.37200	0.87498	5.2791	4.79791	1085	0.58824	0.83776	5.8043	6.08055
1087	0.45956	0.86854	5.6154	4.94110	981	0.56119	0.84323	5.7363	5.78357
1190	0.50888	0.84901	5.5923	4.83735	878	0.53480	0.84907	5.6883	5.53233
1279	0.56395	0.83000	5.6033	4.70988	774	0.50906	0.85525	5.6544	5.31241
1369	0.62539	0.81246	5.7314	4.45957	660	0.48397	0.86174	5.6308	5.11654
1461	0.69468	0.8007	6.6904	3.72960	567	0.45956	0.86853	5.6153	4.94135
$\varepsilon_{min} = -4.54321 + 0.71493 \ln T$ $\varepsilon_{max} = 0.87558 - 0.00088 \ln (T - 575)$ $\lambda_m = 5.27029$ $p = -0.73971 + 0.89432 \ln (T - 500)$					$\varepsilon_{min} = -2.61382 + 0.43705 \ln T$ $\varepsilon_{max} = 1.37626 - 0.07249 \ln T$ $\lambda_m = 5.09496$ $p = 3.46521 + 0.25284 \ln (T - 528)$				

sections with lower temperatures, where sintering does not occur; and (B) for furnace sections with higher temperatures, where sintering does occur, the empirical correlations for $\varepsilon_{min}(T)$, $\varepsilon_{max}(T)$, $p(T)$ and λ_m should be taken solely from the tables related to deposit cooling.

This method can be extended to the other specimens from the same furnace. For each zone of the furnace, that is being thermally designed, appropriate correlations shall be used. The results i.e. the obtained data are applicable to the thermal design of new furnaces – with similar geometry and combusting similar coal – as the existing ones.

However, the proposed method is applicable more generally. It can be used even in cases with totally different boiler furnaces combusting completely different coal. One should just run the whole experiment again but with own – new ash deposit samples. The newly derived data will then be applicable to the thermal design of those new furnaces – having similar geometry and combusting similar coal as in these new experiments.

5. Conclusions and recommendations

In order to facilitate the computation of energy transfer in coal combustion boilers of electric power plants, with strong fouling (ash depositions), an investigation was done (by present authors) on infrared radiation characteristics of coal ash layers. The ob-

Table 6
Parameters: $\varepsilon_{min}(T)$, $\varepsilon_{max}(T)$, $p(T)$ and λ_m, of the function $\varepsilon_H(\lambda,T)$ for Sample 4.

Sample 4									
Heating					Cooling				
T/K	ε_{min}	ε_{max}	λ_m/μm	p	T/K	ε_{min}	ε_{max}	λ_m/μm	p
573	0.03536	0.8976	5.02457	3.65382	1459	0.69499	0.90142	4.8955	10.5124
709	0.20446	0.81403	5.44327	4.80382	1369	0.66598	0.90347	4.9009	10.1299
828	0.24696	0.79663	5.49495	5.25391	1280	0.63818	0.90547	4.9051	9.89147
908	0.26163	0.78083	5.50878	5.19203	1189	0.6123	0.90787	4.9137	9.60327
992	0.29977	0.78092	5.48288	5.49653	1103	0.58545	0.9103	4.9231	9.39420
1107	0.3747	0.79785	5.50541	5.92463	990	0.56065	0.91297	4.9349	9.20551
1190	0.41488	0.77857	5.4251	6.0811	899	0.53681	0.9159	4.9491	8.99741
1281	0.46008	0.75811	5.31352	6.56901	783	0.51338	0.91963	4.9679	8.67203
1370	0.50804	0.74005	5.1851	7.02359	678	0.48536	0.9285	5.0013	7.42808
1459	0.56085	0.72308	5.00731	7.98413	566	0.45899	0.93616	5.0242	6.74736
$\varepsilon_{min} = -2.90056 + 0.46653 \ln T$ $\varepsilon_{max} = 0.8967 - 0.01794 \ln(T - 572.05)$ $\lambda_m = 5.40998$ $p = -0.30734 + 0.95137 \ln(T - 508.0621)$					$\varepsilon_{min} = 1.56966 - 0.16766 \ln T$ $\varepsilon_{max} = 2.31803 - 0.21823 \ln T$ $\lambda_m = 5.39147$ $p = 24.60232 - 2.55958 \ln T$				

tained results were discussed and analyzed from an engineering point of view.

The concluding remarks have been summarized as follows:

- ash deposit layers are opaque for the infrared radiation, and it means that the obtained emittance values are indeed the true properties of deposit surfaces;
- spectral normal emittance continually increases with the increase of wavelength, as well as with the increase of temperature, especially at lower wavelengths;
- above 1200 K ash layers are sintered and fused, and higher density layers are formed that can't possibly reach their initial state by any cooling;
- total emittance decreases with the increase of temperature to the onset of sintering, then increases to the onset of fusion, and in the cooling mode a "hysteresis" is present;
- the value of ε_N in the $\lambda = 2.5$-4 μm wavelength region in the cooling mode is higher than that in the heating mode, as a consequence of ash sintering and – fusion;
- we propose to correlate the experimentally obtained emittance spectra with a single continuous function, Eq. (8), that defines the dependence of ε upon λ and T;
- we suggest a selective use of the temperature dependent parameters in Eq. (8): $\varepsilon_{min}(T)$, $\varepsilon_{max}(T)$, $p(T)$ and λ_m; those bound with "heating" data – only for furnace sections with lower temperature (where deposits can not sinter), and those bound to the "cooling" data – only for furnace sections with higher temperature (where deposits do sinter);
- this technique can be extended to other specimens from the same boiler furnace; the obtained data are applicable to thermal design of new furnaces – with similar geometry and combusting similar type of coal – as the existing furnaces;
- the proposed method is applicable even more generally; with different boiler furnaces combusting different coal; the experiments should be run on own – new deposit samples; these data will then be applicable to thermal design of that new class of furnaces, having similar geometry and combusting similar coal, as in these new experiments.

Acknowledgments

This research was partly supported by Grant-in-Aid for JSPS Fellow (01200058) of Ministry of Education, Science and Technology of Japan. The authors are grateful to Sensei, Prof. Dr. Toshiro Makino, Kyoto Daigaku, for invaluable guidance and support, and to Asst. Prof. Dr. Hidenobu Wakabayashi, Kyoto Daigaku for important assistance.

Special thanks are duly attributed to Mrs. Biljana (Vucicevic) Vucetic, Vinca Institute of Nuclear Sciences, the engineering and computer skills of which have greatly contributed to efficient conduction of the experiments and processing of data.

References

[1] M.F.R. Mulcahy, J. Boow, P.R.C. Goard, Fireside deposits and their effect on heat transfer in a pulverized-fuel boiler: Part I, J. Inst. Fuel 39 (1966) 385–394.
[2] M.F.R. Mulcahy, J. Boow, P.R.C. Goard, Fireside deposits and their effect on heat transfer in a pulverized-fuel boiler: Part II, J. Inst. Fuel 39 (1966) 394–398.
[3] J. Boow, P.R.C. Goard, Fireside deposits and their effect on heat transfer in a pulverized-fuel boiler: Part III, J. Inst. Fuel 42 (1969) 412–419.
[4] V. Mitor, I. Konopel'ko, Issledovanie stepeni chernoty zolovyh otlozhenij i nekotoryh ogneupornyh materialov, Teploenergetika 10 (1970) 41–43 (in Russian).
[5] A. Abrjutin, E. Karasina, Stepen' chernoty i pogloshchateljnaja sposobnost' otlozhenij zoly v topkah kotel'nyh agregatov, Teploenergetika 10 (1970) 43–46 (in Russian).
[6] B. Brajuskovic, M. Uchiyama, T. Makino, Experimental investigation of total emittances of power-plant boiler ash deposits, Exp. Heat Transfer Fluid Mech. Thermodyn. 19 (1991) 605–612.
[7] T.F. Wall, S.P. Bhattacharya, D.K. Zhang, R.P. Gupta, X. He, The properties and thermal effects of ash deposits in coal-fired furnaces, Progress Energy Combust. Sci. 19 (1993) 487–504.
[8] D.G. Goodwin, Infrared optical constants of coal slags, Ph.D. Thesis, School of Mechanical Engineering, Stanford University, Palo Alto, CA, 1986.
[9] G.H. Richards, J.N. Harb, L.L. Baxter, S.P. Bhattacharya, R.P. Gupta, T.F. Wall, Radiative heat transfer in pulverized-coal-fired boilers – development of the absorptive/reflective character of initial ash deposits, in: Proceedings of the 25th Symposium (International) on Combustion, The Combustion Institute, vol. 1, 1994, pp. 511–518.
[10] T.F. Wall, S.P. Bhattacharya, L.L. Baxter, G.H. Richards, J.N. Harb, The character of ash deposits and the thermal performance of furnaces, Fuel Process. Technol. 44 (1995) 143–153.
[11] S.P. Bhattacharya, T.F. Wall, M. Arduini-Schuster, A study on the importance of dependent radiative effects in determining the spectral and total emittance of ash deposits in pulverized fuel furnaces, Chem. Eng. Process. 36 (1997) 423–432.
[12] S.P. Bhattacharya, Apparent emittance of non-isothermal particulate deposits, Int. Commun. Heat Mass Transfer 26 (1999) 771–780.
[13] S.P. Bhattacharya, A theoretical investigation of the influence of optical constants and particle size on the radiative properties and heat transfer in ash clouds and deposits, Chem. Eng. Process. 39 (2000) 471–483.
[14] http://www.ssi.shimadzu.com/products/.
[15] http://www.se.konicaminolta.us/products/.
[16] A. Zbogar, F.J. Frandsen, P.A. Jensen, P. Glarborg, Heat transfer in ash deposits: modelling tool-box, Progress Energy Combust. Sci. 31 (2005) 371–421.
[17] B. Vučićević, Prilog rešavanju problema određivanja ukupne polusferne emisivnosti naslaga stvorenih pri sagorevanju domaćih lignita, Master's thesis, Faculty of Mechanical Engineering, Belgrade University, Belgrade, Serbia, 2004 (in Serbian).
[18] Y. Itaya, N. Nishio, S. Hatano, N. Kobayashi, J. Kobayashi, S. Mori, Near- infrared radiation and scattering properties of coal fly ash particles cloud, J. Chem. Eng. Jpn. 39 (7) (2006) 718–723.
[19] L.L. Baxter, T.H. Fletcher, D.K. Ottesen, Spectral emittance measurements of coal particles, Energy Fuels 2 (1988) 423–430.